



HAL
open science

Nanoparticles Assume Electrical Potential According to Substrate, Size, and Surface Termination

Stepan Stehlik, Tristan Petit, Hugues Girard, Jean-Charles Arnault,
Alexander Kromka, Bohuslav Rezek

► **To cite this version:**

Stepan Stehlik, Tristan Petit, Hugues Girard, Jean-Charles Arnault, Alexander Kromka, et al.. Nanoparticles Assume Electrical Potential According to Substrate, Size, and Surface Termination. Langmuir, 2013, 29, pp.1634-1641. 10.1021/la304472w . cea-01816682

HAL Id: cea-01816682

<https://cea.hal.science/cea-01816682v1>

Submitted on 21 Feb 2025

HAL is a multi-disciplinary open access archive for the deposit and dissemination of scientific research documents, whether they are published or not. The documents may come from teaching and research institutions in France or abroad, or from public or private research centers.

L'archive ouverte pluridisciplinaire **HAL**, est destinée au dépôt et à la diffusion de documents scientifiques de niveau recherche, publiés ou non, émanant des établissements d'enseignement et de recherche français ou étrangers, des laboratoires publics ou privés.

Nanoparticles Assume Electrical Potential According to Substrate, Size, and Surface Termination

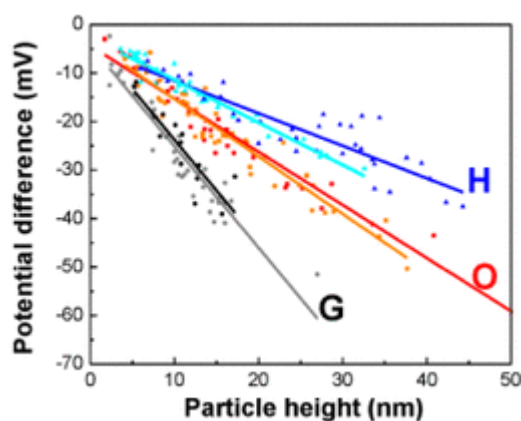
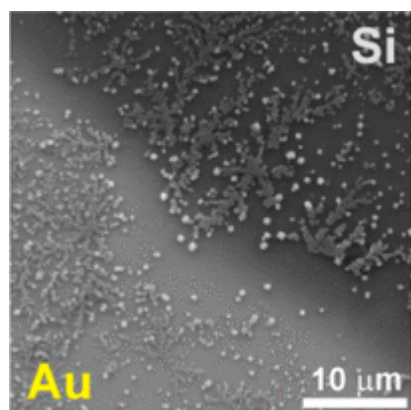
Stepan Stehlik ^{1,*}, Tristan Petit ², Hugues A. Girard ², Jean-Charles Arnault ², Alexander Kromka ¹, Bohuslav Rezek ¹

¹ Institute of Physics, Academy of Sciences of the Czech Republic, v.v.i., Cukrovarnická 10, 162 00, Prague 6, Czech Republic

² CEA, LIST, Diamond Sensors Laboratory, F-91191 Gif-sur-Yvette, France

Abstract

Electrical potential of nanoparticles under relevant environment is substantial for their applications in electronics as well as sensors and biology. Here, we use Kelvin force microscopy to characterize electrical properties of semiconducting diamond nanoparticles (DNPs) of 5–10 nm nominal size and metallic gold nanoparticles (20 and 40 nm) on Si and Au substrates under ambient conditions. The DNPs are deposited on Si and Au substrates from dispersions with well-defined zeta-potential. We show that the nanoparticle potential depends on its size and that the only reliable potential characteristic is a linear fit of this dependence within a 5–50 nm range. Systematically different potentials of hydrogenated, oxidized, and graphitized DNPs are resolved using this methodology. The differences are within 50 mV, that is much lower than on monocrystalline diamond. Furthermore, all of the nanoparticles assume their potential within –60 mV according to the Au and Si substrate, thus gaining up to 0.4 V difference. This effect is attributed to DNP charging by charge transfer and/or polarization. This is confirmed by secondary electron emission. Such effects are general with broad implications for nanoparticles applications.



Introduction

Nanoparticles of diverse materials and sizes represent an emerging type of materials that find nowadays broad use in commercial products as well as attract attention in fundamental research with a perspective of greatly improved or completely new effects.

There are numerous analytical techniques to characterize the properties of nanoparticles. The atomic structure can be resolved by high resolution transmission electron microscopy (HRTEM), the surface chemistry by X-ray photoelectron spectroscopy (XPS), or infrared and Raman spectroscopies and colloidal properties by dynamic light scattering (DLS). These techniques require sophisticated

equipment with careful sample preparation (HRTEM) or do not resolve single particles and thus provide only average information of a sample (XPS, zeta potential (ZP) measurement). To our knowledge, no measurements of electrical potential of individual nanoparticles on two or more different surfaces have been reported although it represents a fundamental property for many interactions and applications.

Scanning probe techniques, in particular Kelvin force microscopy (KFM) proved to be sensitive tool for chemical and electrical characterization of numerous materials, nanostructures, and junctions. Because of high spatial resolution and sensitivity of the work function to chemical condition of surfaces, KFM measurements can provide valuable insight into the surface chemistry of nanoscale structures and objects. This method combines atomic force microscopy (AFM) with the Kelvin probe technique. It is based on vibrating parallel plate capacitor formed by a sample and AFM tip. Because of the difference in the work function (Φ) of the two materials a contact potential difference (CPD) arises.

$$V_{CPD} = \frac{\Delta\Phi}{e} = \frac{(\Phi_{sample} - \Phi_{tip})}{e} \quad (1)$$

The CPD is then compensated by external voltage applied to one of the plates (tip or sample) which enables quantitative mapping of surface potential with nanometer resolution if the work function of the tip is known. (1) The work function is defined as follows:

$$\Phi = E_{vac} - E_F \quad (2)$$

where E_{vac} is energy of vacuum level and E_F represents the Fermi energy of electrons.

KFM has been successfully used for potential mapping of monocrystalline and nanocrystalline diamond with various surface terminations. On the basis of different work function and thus potential of hydrogenated and oxidized diamond surface KFM clearly distinguished areas with different surface termination although topography showed no difference. (2, 3) Moreover, KFM can be used to recognize covalent grafting of organic molecules to the diamond surface. (4) However, correct determination of a nanostructure electrical potential is not straightforward. Salem et al. (5) reported a dependence of potential on the height of silicon nanocrystals embedded in Si/SiO₂ matrix as well as their intentional charging by the AFM tip. This led to inversion of KFM contrast of the nanoparticles vs substrate. Dependence of potential on the height of a nanostructure was observed also on other systems on atomic scale in ultrahigh vacuum (UHV). (6, 7) Theoretical studies also showed dependence of nanoparticles penetration ability through cell membranes on their shape and charge. (8)

In addition to the size dependence, the work function of a surface is strongly affected by the surface state. Very small amounts of contamination or the occurrence of surface reactions can substantially alter the work function of a surface. These changes result from formation of electric dipoles at the surface, which change the energy an electron needs to reach the vacuum level. Controlling and properly characterizing the state of surface (chemical, structural, electronic) is thus fundamental for understanding and applying properties of nanoparticles and other nanostructures.

Here, we employ diamond nanoparticles (DNPs) and gold nanoparticles (GNPs) as practical representatives of semiconducting and metallic nanoparticles that are available in colloidal solutions. At the same time, both types of nanoparticles represent typical nanomaterials with interesting properties and broad application potential.

Diamond nanoparticles are gaining considerably increasing interest due to their specific properties and application potential in biology, medicine, (9) chemistry as well as nanoscale physics. (10) Formation of DNPs by detonation has been first reported in 1961. (11) Nowadays DNPs are available in large quantities although their quality may differ. Thanks to their stable diamond core combined with a

tunable surface chemistry, (12) DNPs now possess high application potential in many fields, going from biology (fluorescence imaging, (13) drug delivery (14, 15)) across sensors (surface acoustic wave sensors, (16) sensitive chemical sensors (17)), single photon sources (18, 19) to the application of DNPs in neutron physics. (20) In all these applications DNPs offer unique properties such as: biocompatibility, various possibilities of surface functionalization, (21) presence of impurities (NV⁻ and other color centers), and low absorption cross section of very cold neutrons. Partially graphitized DNPs with fullerene-like reconstruction on their surfaces or fully graphitized DNPs which are known as OLCs (onion-like carbon) are perspective nanomaterials for supercapacitors. (22, 23) DNPs are also indispensable for chemical vapor deposition of nanocrystalline diamond where they serve as seeds for growth on diverse substrate materials and morphologies. (24-27)

Gold nanoparticles have attracted interest of scientist since a long time. Besides being the model material for study of quantum size effects, for example plasmon resonance, single electron transitions, and quantized capacitance charging or serving as nanoscale contacts to molecules, they are also broadly used in various biomedical applications due to their large surface area to volume ratio, high reactivity with the living cells and stability over high temperatures, and so forth. The properties and various applications of GNPs are regularly reviewed. (28, 29)

In this work, we show that the potential of both diamond and gold nanoparticles depends on their size and surface chemistry in somewhat unexpected manner. Moreover, fundamental influence of substrate on a nanoparticle potential is revealed and discussed.

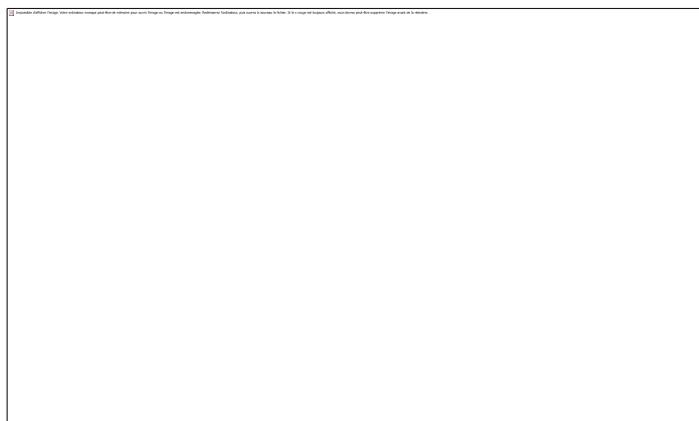
Experimental Section

As the DNPs we used ultradispersed detonation nanodiamonds provided by the NanoCarbon Research Institute Co., Ltd. (Japan) with nominal size of 5 nm. To achieve the desired surface termination, the DNPs were treated as follows: by microwave enhanced plasma hydrogenation (20 min, H₂ pressure of 15 mbar, microwave power of 300 W) to achieve H-terminated surface (H-DNPs) (30, 31) annealed 1h in vacuum at 750 °C to obtain partially graphitized surface (G-DNPs), (32) and annealed 4h in air at 400 °C to obtain oxidized surface (O-DNPs). (33) The DNPs were then dispersed in water by sonication (Hielscher UP400S, 300W, 24 kHz) for 2h under cooling. Oxidized DNPs had negative zeta potentials while hydrogenated and graphitized DNPs had positive zeta potential at same pH. The H-DNPs were also dispersed in methanol for KFM experiments to avoid certain tendency to aggregate in water. The dispersed DNPs were deposited on n-type Si wafers (10 Ω.cm) with Ti/Au (10/50 nm) electrodes by drop-casting using micropipet and letting dry. The concentration of the DNP dispersions was optimized manually to deposit scattered particles rather than continuous layers on the substrates. For comparison, colloidal gold nanoparticles were employed. We used 20 and 40 nm GNPs (BBI), which were deposited on the above-mentioned Au/Si substrates. The adherence of the GNPs toward Au/Si substrate was enhanced by addition of 1.2 μL of 5% HF to the 1 mL of the original colloidal solution. (34) The substrate was left in such prepared solution for 10 min to achieve proper coverage.

Hydrodynamic diameters and zeta potentials of the particles were performed in ultrapure water on a Nanosizer ZS (Malvern) in the back scattering configuration (173°). All experiments were performed with the manufacturer calibration procedures. The average value of at least five measurements was taken at a given condition.

Kelvin force microscopy was performed by a scanning probe microscope (N-TEGRA system by NT-MDT) under ambient conditions (room temperature, 23–25 °C; and low relative humidity, 20–30%). Two-pass KFM technique with amplitude modulation was used. We used conductive silicon probes (Multi75Al-G, Budgetsensors) with high level of doping (0.01–0.025 Ω.cm), with nominal tip radius of 10 nm and spring constant of 3 N/m. The set-point ratio was kept at 0.6 of the free oscillation

amplitude (60 nm) in the first pass. The ac oscillation voltage in the second pass was 5 V and the tip-sample offset was $\Delta z = 5$ nm. All the parameters were kept constant for all the KFM measurements. The KFM setup for measurement of DNPs on Au and Si substrates is schematically shown in the Scheme 1.



Scheme 1. Schematic Drawing of the Kelvin Force Microscopy (KFM) Setup for Characterization of Diamond and Gold Nanoparticles on Au and Si Substrates

XPS analysis was performed using a monochromatized Al K α anode (1486.6 eV) calibrated versus the Au 4f $_{7/2}$ peak located at 84.0 eV. The spectrometer was equipped with an EA 125 hemispherical analyzer. The path energy was 20 eV corresponding to an absolute energy resolution of 0.6 eV. The detection limit of our XPS setup is of 0.5 at. %. Areas of XPS core levels were extracted after a Shirley correction of the background and atomic contents are calculated after correction by the photoionization cross sections.

To characterize secondary electron emission from the samples, field-emission scanning electron microscope (SEM) (MIRA3, TESCAN) was operated with InBeam detector using 5 kV acceleration voltage.

Results

The surface chemistry of each modified DNPs was studied by XPS. In Figure 1 the XPS C1s spectra of the three DNPs are plotted. The oxygen content of the O-DNPs is 12.8 at. % showing that these DNPs are indeed well oxidized. The C1s is broad (fwhm = 3.2 eV) and shifted toward high binding energy (max at 290.0 eV) due to C-O and C=O bonds but also due to charging effects coming from the insulating behavior of O-DNPs.

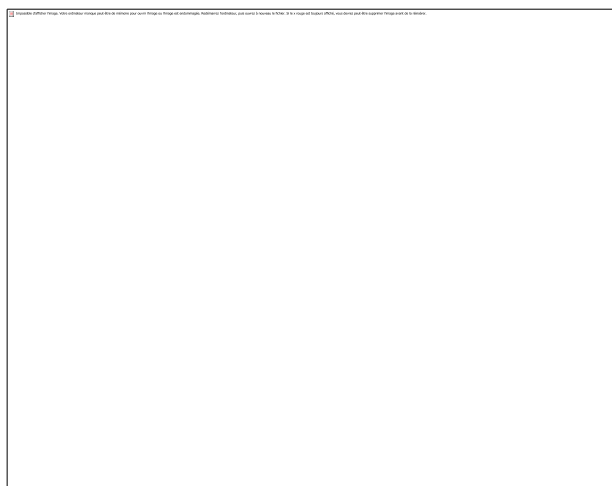


Figure 1. XPS C1s spectra of O–DNPs, H–DNPs, and G–DNPs after in situ annealing at 400°C.

H–DNPs and G–DNPs are very sensitive to air contamination. (12, 30) Therefore, the related XPS spectra were recorded after 1 h in situ annealing at 400 °C to remove adsorbates. The remaining oxygen contents after annealing are 1.2 and 2.9 at. % for H–DNPs and G–DNPs, respectively (compared to 2.7 and 6.3 at. %, initially). For H–DNPs, the C1s spectra exhibit a narrow peak at 286.9 eV (fwhm = 1.4 eV) showing that no amorphous, graphitic carbon, or oxygen groups are detected on the surface. For G–DNPs, the C1s peak is broader (fwhm = 2.2 eV) and a shoulder at 284.8 eV is clearly visible. This is a characteristic feature of sp² carbon, in agreement with HR-TEM characterization. (12)

After dispersion in water, size distributions of modified DNPs were measured by DLS (part a of Figure 2). Mean diameters in O–DNPs and G–DNPs dispersions correspond to 10 nm, which is close to the diameter of the primary particles (5 nm). For H–DNPs, a certain aggregation is observed in water dispersions, with mean diameters between 30 and 40 nm.

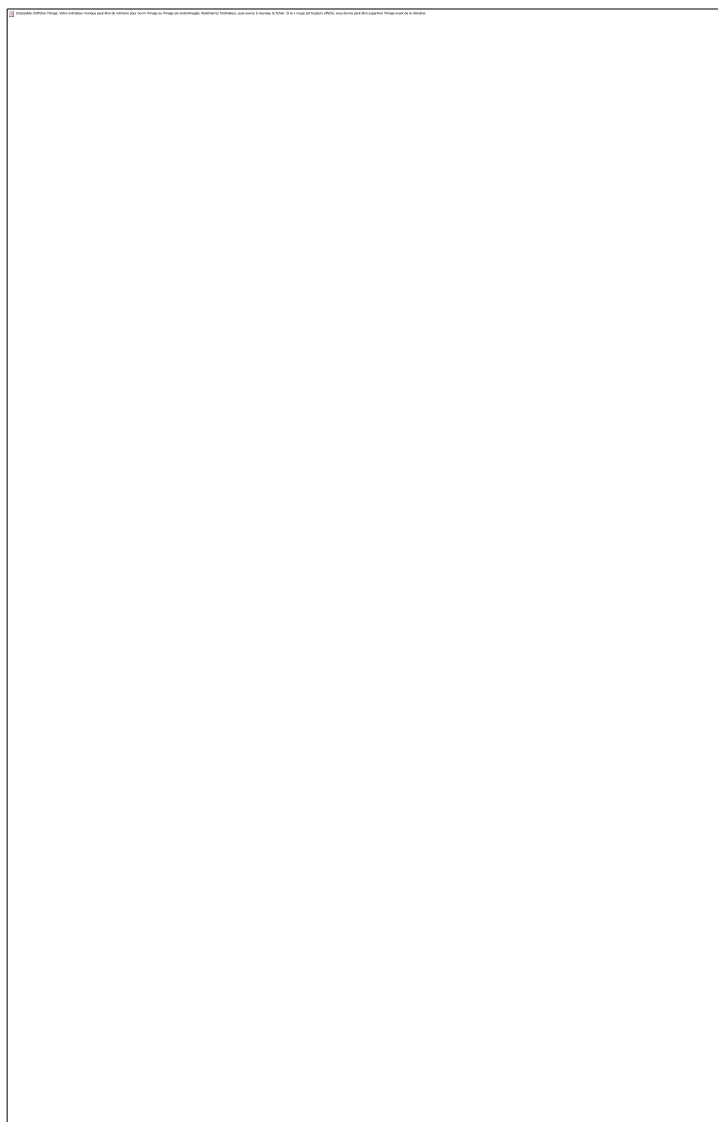


Figure 2. Size distributions measured by DLS (a) and zeta potential evolution (b) for each modified DNPs.

The zeta potential of the three types of DNPs are plotted in part b of Figure 2 as a function of pH. Particular pH was adjusted by 0.1 M NaOH and HCl. O–DNPs have indeed negative ZP over the full range of pH, whereas G–DNPs and H–DNPs have positive ZP up to pH 12.

The typical AFM topography with corresponding KFM map of the oxidized DNPs on Si substrate is shown in Figure 3. Single DNPs of 5 nm height as well as aggregates with height ranging up to 50 nm are observed. Note, that lateral DNPs dimensions are overestimated since the AFM image (part a of Figure 3) is influenced by a convolution of the sample and the tip shape. Thus we estimate the DNP sizes from the AFM height. DNPs are well visible also in the KFM image (part b of Figure 3) as dark spots. The potential of nanoparticles is not constant but varies with the size. It is thus difficult to assign a characteristic potential to a particular DNP. This is even more obvious from corresponding histograms. Whereas the topography histogram clearly shows the maximum corresponding to substrate as well as the tail related with distribution of the particle heights, the KFM histogram shows no characteristic value corresponding to DNPs.

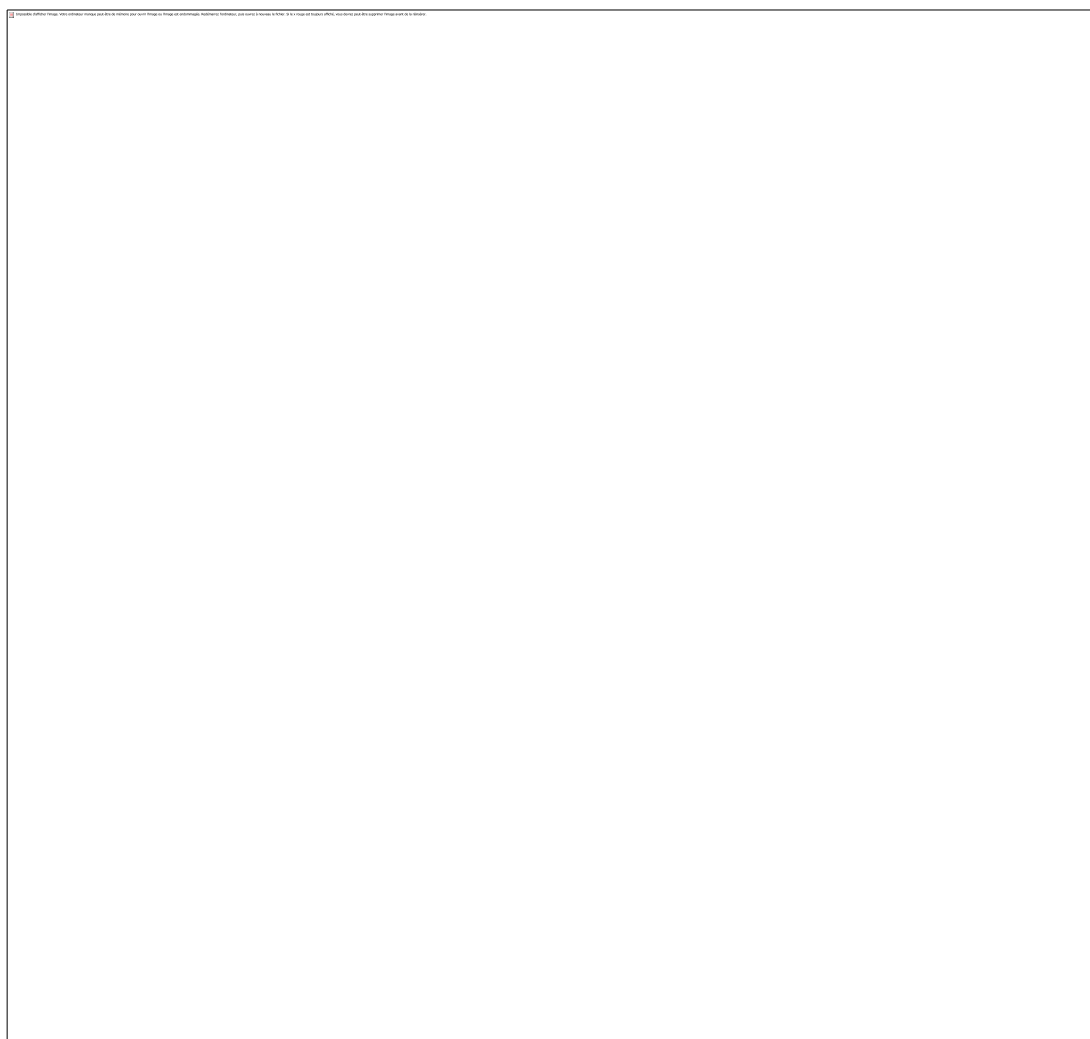


Figure 3. AFM topography image (color range 55 nm) of a $2 \times 2 \mu\text{m}^2$ area of oxidized DNPs on Si substrate (a). Corresponding KFM signal (color range 120 mV) on oxidized DNPs on Si substrate (b). Corresponding histograms of height and potential are shown below the images.

To investigate a variation of the potential with the size of DNPs, we plotted potential as a function of DNPs height on Au and Si substrates in part a of Figure 4. The data has been extracted from the

AFM/KFM images such as those in Figure 3. We can see that the height dependence of the potential shows a clear trend that can be fitted well by a linear regression in the range of recorded sizes. Rather narrow 95% confidence bands indicate relatively high accuracy of the linear fit. Note, that the potential difference of ~ 425 mV corresponds to the difference of work function between Au and Si substrates.

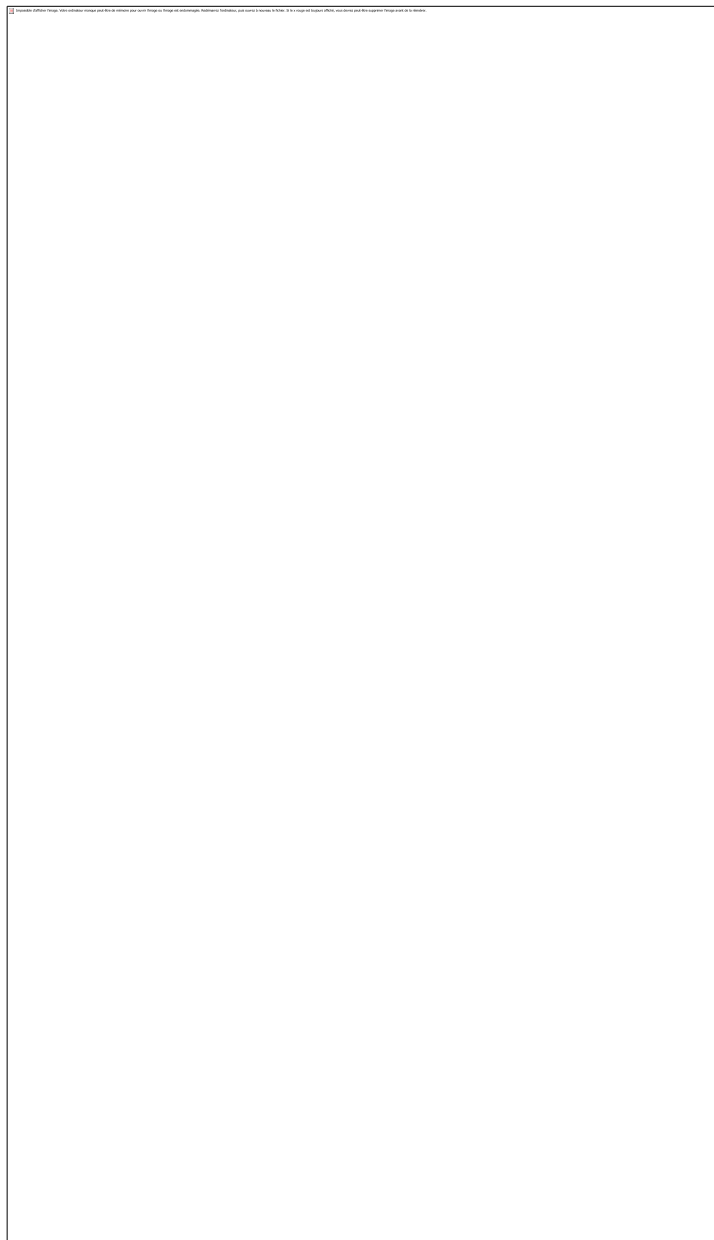


Figure 4. Potential of oxidized DNPs as a function of particle height on Au (orange) and Si (red) substrates showing very similar potential evolution on both Au and Si substrates (a). The lines correspond to a linear regression fit with 95% confidence bands. The potential offset is due to the work function difference between the substrates. Potential difference of DNPs vs Au and Si substrates as a function of particle height (b). The data for hydrogenated (triangles), oxidized (squares), and graphitized (circles) DNPs are shown.

We applied this approach to the all three types of DNPs with different surface termination and we subtracted potential of both substrates from the DNPs gaining the potential difference vs substrate as

the function of their heights. These data are summarized in part b of Figure 4. Several fundamental facts can be observed in part b of Figure 4. First, the slope of the linear fit depends on surface termination of DNPs. Thus by using the potential-height analysis, KFM is able to reliably distinguish among the different types of DNPs, although the effect of surface termination is relatively small (within 50 mV). Second, the slope of the linear fit is surprisingly very similar both on Au and on Si for all three types of DNPs. It seems that the DNPs follow the potential of the substrate. This observation was independently confirmed by SEM. The SEM image of oxidized DNPs taken in the secondary electron regime is shown in the part a of Figure 5. Continuous dense layer of the DNPs was formed on the Si/Au substrate and the substrate surface was revealed again in a local area by a gentle scratch using plastic tweezers. Estimated thickness of the layer was about 100 nm. It is obvious that the DNP layer appears brighter both on Au and Si, but its brightness depends on the type of underlying substrate. When we analyze brightness of the DNP layer we can see a clear contrast between the same DNPs residing on Au and on Si (histogram in part b of Figure 5). This confirms that the DNPs accommodate to a potential of a substrate.

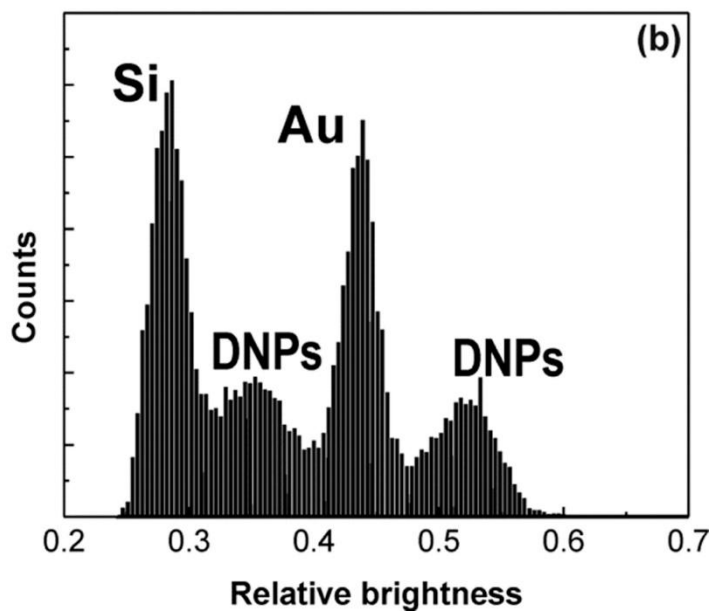
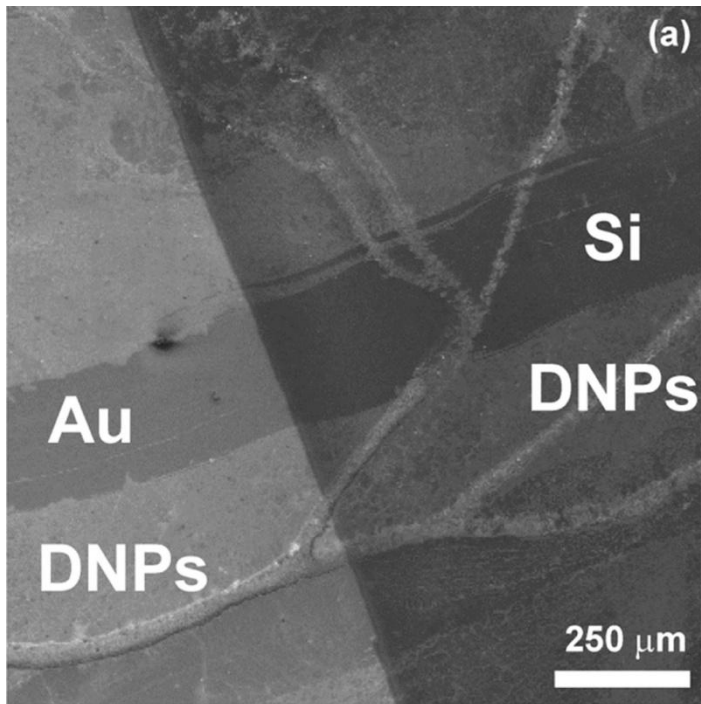


Figure 5. SEM image of the scratched layer of oxidized DNPs on Au/Si substrate (a). Histogram extracted from the SEM image showing the brightness difference of the DNPs vs Au and Si substrates (b).

To verify a general nature of this effect we have investigated gold nanoparticles as a model nanomaterial. Figure 6 shows the dependence of potential difference vs substrate on the particle height for Au nanoparticles as extracted from AFM/KFM data. The linear regression fits with 95% confidence bands are also presented. The insert shows a typical AFM morphology of a substrate (Si) with deposited 20 nm Au nanoparticles. It is fundamental that the graph reveals the same effect as observed for DNPs. Also, the Au nanoparticles accommodate their potential according to size and substrate they reside on. Relative potential difference to the substrate is within 60 mV for both Si and Au substrates. Thus, there is again large absolute potential difference of up to 0.4 V between the same nanoparticles on different substrates.

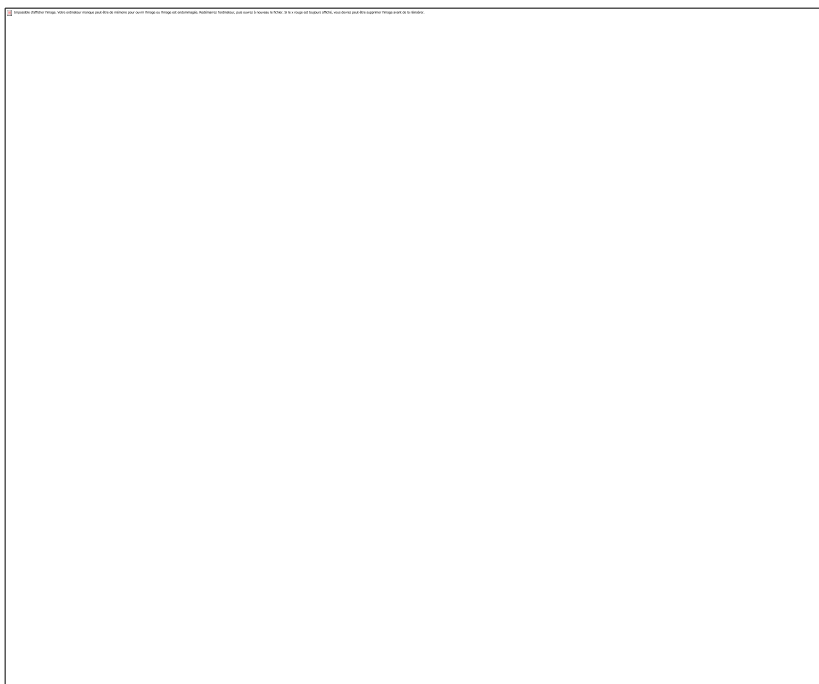


Figure 6. Potential difference of Au nanoparticles vs Au and Si substrates as a function of particle height. The lines correspond to a linear regression fit with 95% confidence bands. The AFM topography image of the 20 nm Au nanoparticles deposited on Si is shown as the inset in the figure. The scan size is $2 \times 2 \mu\text{m}$ and color range is 35 nm.

Discussion

Nominal size of DNPs prepared by detonation process is typically 5–10 nm. Nevertheless, such nanoparticles tend to aggregate into larger clusters and it takes some effort to disperse them well in solution. The DLS and AFM height data indicate that in this study both individual DNPs and small aggregates (below 50 nm) of these DNPs are investigated. Mild aggregation is actually an advantage in our case, since it enables us to collect values of potential as a function of particle/aggregate height.

The XPS results (Figure 1) are good indication of different surface termination of the DNPs. In such treated DNPs, the effect of different chemical moieties and reconstruction is expected to influence the surface properties of DNPs and even their electrical properties. For instance, the difference in surface charge in deionized water is clearly demonstrated by opposite ZP of the oxidized DNPs vs graphitized and hydrogenated DNPs. However, we cannot directly compare the ZP data with the real surface potential obtained by KFM under ambient conditions. It is well-known that contamination and high humidity may partially or fully screen the KFM contrast. (35) Nevertheless, with the measurements conditions kept constant the results were reproducible when measured with different tips of the same kind. This is in agreement with narrow confidence bands of the potential-height trends (part a of Figure 4). In addition we assume that under our conditions a possible contamination is similar on all samples and not detrimental to the KFM measurements, such as in the case of other similar KFM experiments on diamond in air. (2) This is again confirmed by the reproducibility of the experiments. Thus, comparison of the KFM data is reasonable.

For all types of surface terminations, the potential contrast depends on the DNP aggregate size (we assume that the aggregate height in AFM is a reasonable characteristic of its size). Obviously, as evidenced by the smeared histogram of potentials in part b of Figure 3 and by the potential height dependence in Figure 4, one cannot assign a single characteristic potential to the DNPs with particular

surface termination. Instead, we suggest that the reliable potential characteristic of particular DNPs on any substrate is the linear slope of potential-height dependence as obtained from linear regression. Thereby, potentials of differently functionalized nanoparticles can be reliably compared at a selected fixed height.

To explain the height dependence of the potential we consider several factors. Similar height dependence of potential has been reported for other nanoscale objects such as InAs quantum dots (QD) on GaAs (001) substrate and interpreted in terms of the quantum size effect by which the amount of charges accumulated in the QD is determined through the confinement energy levels in the QD. (7) Such effects were limited to sizes below 7 nm. If we exclude quantum confinement effects, a bulk material property (work function) should determine the potential of DNPs with particular surface termination. Work function was found to change by up to 0.1 eV as function of metal layer thickness until 10 nm. (36) In the case of dielectric NaCl film on Cu (111), work function changed by as much as 0.6 eV before saturation at 4 monolayer thickness. (6)

The two above phenomena may come into effect in individual DNPs (5–10 nm size), but they can hardly account for the potential development of larger DNP aggregates. One would rather expect a constant potential corresponding to the work function of DNPs with particular surface termination such as in the case of bulk diamond. (2, 3) Similarly, even if the potential was due to a property of individual DNPs inside the clusters, it should not change with size. However, in the size range of the DNPs and their clusters (5–50 nm) we did not observe any indication of such saturation.

Some contribution to the KFM data may come from stray capacitance between the AFM tip and substrate area surrounding the DNP aggregate. The stray capacitance may lead to potential averaging that is known to influence KFM measurements across material boundaries or nanoscale features. (37, 38) The potential contrast may be reduced by as much as 50% due to the stray capacitance of the AFM tip and cantilever. (39) We have tested increase in the tip-DNP separation from 5 nm (standard value optimized for the best contrast and stable measurements) up to 70 nm during KFM measurement. As expected the increased separation indeed reduced the potential difference vs substrate until it almost disappeared due to reduced local capacitance. However, this effect leads only to overall decrease in the potential difference and it does not influence the observed trend. We have also tested KFM on oxidized DNPs in a frequency-modulated regime, which enables much higher spatial resolution down to atomic scale, (40) and we obtained similar potential differences as in Figure 4. Thus, the stray capacitance has only limited influence on our KFM data.

The potential-height dependence must be thus related with some other property of the nanoparticles. Characterization of DNP potential on different substrates can be used to obtain further insight. Approximate values of work function of the employed substrate materials are Au = 4.9 ± 0.1 eV and Si = 4.6 ± 0.1 eV. By KFM we measured average difference of about 310 ± 30 mV (maximum 460 mV) between Au and Si. Thus, we would expect to see only negligible potential contrast of the H-DNPs on Au as previously shown on hydrogen terminated bulk diamond (2) but substantial contrast versus Si. However, as shown in Figure 4, the potential difference of the DNPs with specific surface termination is independent of the substrate material, Si and Au in our case. This is reproducibly obtained for all three types of surface terminations.

Note that the same potential difference versus Au and Si means that the same DNPs actually have different absolute potential on each substrate. In other words, the DNPs assume potential of the substrate on which they reside. Thus, whereas the difference versus substrate is always within 50 mV, absolute potential difference is up to 0.4 V in the case of our substrates. As discussed above, this effect cannot be explained either by mere averaging of potential due to stray capacitance nor by work function development as a function of material thickness. Because the DNP potential changes on

different substrates, it cannot be only due to DNP work function itself, which is a fixed material parameter and thus should provide only one potential value irrespective of substrate. Therefore, the only other possibility is some kind of additional electrostatic charging of the DNPs. This assertion is independently confirmed by SEM (Figure 5). The layer of the same DNPs follows the secondary electron emission of the substrate, thus it appears brighter on Au than on Si. Although the SEM results can be considered only in a qualitative manner they simply evidence a charge exchange between the DNPs and the substrate and independently support the results obtained by KFM. The charging of DNPs can be realized via transfer of charge to/from nanoparticles or nanoparticle polarization on the substrate. Charge trapping on DNPs may be the dominant effect, because oxidized diamond surfaces exhibit large density of surface states that can even pin the Fermi level. (2, 41, 42) Graphitized nanoparticles may also accommodate some charge in the sp^2 phase as evidenced on nanocrystalline diamond thin films (43) and onion-like carbons (OLCs). (23) In the case of H-terminated diamond the surface states are mostly passivated. Yet some surface states (in density typically below 10^{11} cm^{-2}) may still remain (44) and/or some structural defects may exist in the DNPs prepared by detonation. Nevertheless, further research is still needed to elucidate the details of the charging mechanism.

In spite of all of the effects discussed above, we could resolve that the potential of DNPs is influenced by their surface terminations. In Figure 4, the linear slope of potential difference vs substrate increases and DNPs become generally more negatively charged in the sequence of hydrogenation, oxidation, and graphitization. This discrimination is independent of the employed substrate, which is a beneficial side-effect of the DNPs potential being accommodated to the substrate. Yet note that for reliable comparison it is essential to apply linear regression fit to the height-dependent potential data. Using just some random nanoparticles irrespective of their size might in principle lead to even seemingly opposite trend in the potentials.

If we compare nanoparticle potentials at a fixed height, O-terminated DNPs have more negative potential than H-terminated DNPs. This is in a good correlation with the properties of monocrystalline intrinsic diamond. On monocrystalline intrinsic diamond surfaces a potential difference of up to 0.3 V between H- and O-terminated areas has been detected by KFM. (2, 3, 45) Furthermore, it has been shown that the potential difference between H-terminated diamond surface and Au reference contact is negligible. (2) On the other hand, the O-terminated diamond surface exhibited considerably lower potential versus Au and H-terminated surface. Understanding of this difference is not straightforward in particular due to high electrical resistance of O-terminated intrinsic diamond. On the basis of detailed analysis and assembly of energetic band diagrams, the lower potential was interpreted as a higher work function of the oxidized diamond surface. (3) However, the potential difference between DNPs as a function of surface termination is small, within 50 mV, compared to the values found on the bulk diamond. The reason is most likely the additional charging of the nanoparticles as discussed above.

Similarly we can deduce properties of graphitized DNPs that represent new but rather complicated nanosystem. (12) As they exhibit more negative potentials, the graphitized DNPs may have higher work function than the other two terminations. Indeed, nanoscale graphitic patches of higher work function were suggested as possible source of carriers that are then emitted via H-terminated sites on monocrystalline diamond. (46) However, it is also possible that the graphitized DNPs can store considerable amount of charge such as in the case of nanocrystalline diamond films where charging of sp^2 phase dominated over the charging and polarization of diamond grains. (43, 47) Also, OLCs synthesized by full graphitization of detonation nanodiamonds have shown remarkable charge storage capabilities in supercapacitors. (23) Nevertheless, we assume that the potential differences between the DNPs with various surface terminations are determined mostly by their work functions, in spite of overall charging that accommodates their potential to the particular substrate.

On the basis of the above discussion we propose the energetic scheme that is depicted in the Figure 7. Because the DNPs do not keep their own potential we cannot assign the real value of potential to particular kind of DNPs. The scheme rather shows relative differences between silicon AFM tip and DNPs with various surface terminations. The levels of DNPs are spread to indicate potential variation as a function of size. On the relative scale shown here, the trend and discrimination between various surface terminations is most likely governed by work functions of functionalized DNPs because the amount charging is obviously significantly different on Au and Si substrates. The relative trend is general, independent of the substrate. However, quantitatively the potential of nanoparticles is influenced by the electrostatic charging and/or polarization of the DNPs on the substrate.

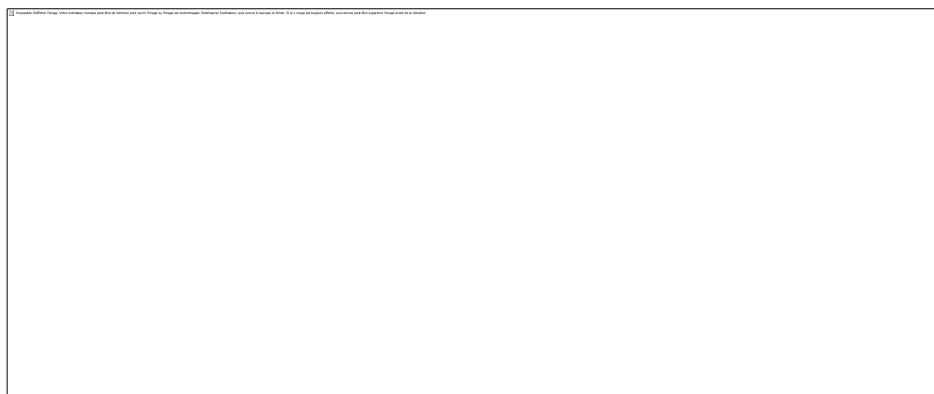


Figure 7. Energetic scheme showing relative differences between silicon AFM tip and DNPs with various surface terminations. The levels of DNPs are spread to indicate potential variation as a function of size.

As obvious from Figure 6, all of above arguments and conclusions are valid also for GNPs. The GNPs assume potential according their size and the substrate in the similar range of potentials as the diamond nanoparticles. This confirms that even for the GNPs the electrical potential is strongly influenced by the substrate. In the case of GNPs, this effect may be influenced by surfactants (citrate) that stabilize the GNPs colloidal solution and may reside on the surface of a GNP. Also nanoscale dimensions may play substantial role. (48) For example superior catalytic activity of GNPs (49) compared to poor catalytic performance of bulk gold has been demonstrated. This suggests different properties of GNPs compared to bulk gold. Further research is needed to elucidate details of these effects. Nevertheless, on the basis of the above facts and arguments we suggest that the described phenomena related with electrical potential of nanoparticles on surfaces are general and applicable to many kinds of nanoparticles, metallic, semiconducting, or insulating.

Conclusions

On the basis of our data and arguments, we conclude that the reliable potential characteristic of a nanoparticle on any substrate is the slope of potential-height dependence as obtained from linear regression. Potentials of different nanoparticles can be thereby reliably compared at a given size. Potential differences versus substrate are about the same on both Au and Si substrates. Even the slopes of potential-height dependencies are similar. It suggests that the potential of a nanoparticle is not given by its material properties but it assumes potential of the substrate. This was independently confirmed by SEM where the secondary electron emission from the nanoparticles was strongly affected by the substrate in a similar manner. We attributed this effect to electrostatic charging and polarization of the nanoparticles. To the best of our knowledge, this is the first investigation of an identical nanostructure on two or more substrates by KFM. On the basis of comparison of diamond and gold nanoparticles, this effect is most likely general for all kinds of nanoparticles and nanoscale objects. In spite of the above effects, systematically different potentials of hydrogenated, oxidized, and graphitized DNPs were resolved using our methodology. In our opinion, the presented results are fundamental for understanding and applications of nanoparticles and provide foundation for such studies also on other nanoscale materials.

Notes

The authors declare no competing financial interest.

Acknowledgment

Technical support Jitka Libertínová and Martin Müller is gratefully appreciated. Matthias Fenner from Agilent Technologies is acknowledged for FM-KFM testing measurements. Authors thank Prof. E. Osawa for providing DNPs. This research was financially supported by the projects P108/12/G108 (GACR) and M100100902 (AVCR). This work occurred in frame of the LNSM infrastructure.

References

1. Sadewasser, S. Experimental technique and working modes. In Kelvin Probe Force Microscopy; Sadewasser, S., Glatzel, T., Eds.; Springer-Verlag: Berlin Heidelberg, 2012; pp 7–24.
2. Rezek, B.; Sauerer, C.; Nebel, C. E.; Stutzmann, M.; Ristein, J. Fermi level on hydrogen terminated diamond surfaces *Appl. Phys. Lett.* **2003**, *82*, 2266
3. Rezek, B.; Nebel, C. E. Kelvin force microscopy on diamond surfaces and devices *Diam. Relat. Mater.* **2005**, *14*, 466–469
4. Čermák, J.; Rezek, B.; Kromka, A.; Ledinský, M.; Kočka, J. Electrochemical synthesis and electronic properties of polypyrrole on intrinsic diamond *Diam. Relat. Mater.* **2009**, *18*, 1098–1101
5. Salem, M. A.; Mizuta, H.; Oda, S. Probing electron charging in nanocrystalline Si dots using Kelvin probe force microscopy *Appl. Phys. Lett.* **2004**, *85*, 3262
6. Glatzel, Th.; Zimmerli, L.; Koch, S.; Such, B.; Kawai, S.; Meyer, E. Determination of effective tip geometries in kelvin probe force microscopy on thin insulating films on metals *Nanotechnology* **2009**, *20*, 264016
7. Yamauchi, T.; Tabuchi, M.; Nakamura, A. Size dependence of the work function in InAs quantum dots on GaAs(001) as studied by Kelvin force probe microscopy *Appl. Phys. Lett.* **2004**, *84*, 3834

8. Nangia, S.; Sureshkumar, R. Effects of Nanoparticle charge and shape anisotropy on translocation through cell membranes *Langmuir* **2012**, *28*, 17666– 17671
9. Schrand, A. M.; Ciftan Hens, S. A.; Shenderova, O. A. Nanodiamond particles: properties and perspectives for bioapplications *Crit. Rev. Solid State* **2009**, *34*, 18– 74
10. Mochalin, V. N.; Shenderova, O.; Ho, D.; Gogotsi, Y. The properties and applications of nanodiamonds *Nature Nanotechnol.* **2012**, *7*, 11– 23
11. De Carli, P. J.; Jameieson, J. C. Formation of diamond by explosive shock *Science* **1961**, *133*, 1821– 1822
12. Petit, T.; Arnault, J. C.; Girard, H. A.; Sennour, M.; Kang, T.-Y.; Cheng, C.-L.; Bergonzo, P. Oxygen hole doping of nanodiamond *Nanoscale* **2012**, *4*, 6792
13. Takimoto, T.; Chano, T.; Shimizu, S.; Okabe, H.; Ito, M.; Morita, M.; Kimura, T.; Inubishi, T.; Komatsu, N. Preparation of fluorescent diamond nanoparticles stably dispersed under a physiological environment through multistep organic transformations *Chem. Mater.* **2010**, *22*, 3462– 3471
14. Lam, R.; Ho, D. Nanodiamonds as vehicles for systemic and localized drug delivery *Expert Opin. Drug Deliv.* **2009**, *6*, 883– 95
15. Huang, H.; Pierstorff, E.; Liu, K.; Osawa, E.; Ho, D. Nanodiamond-mediated delivery of therapeutics via particle and thin film architectures. *Nanodiamonds: Applications in Biology and Nanoscale Medicine*; Ho., D., Ed.; Morwell: Springer; pp 151– 174.
16. Chevallier, E.; Scorsone, E.; Girard, H. A.; Pichot, V.; Spitzer, D.; Bergonzo, P. Metalloporphyrin-functionalised diamond nano-particles as sensitive layer for nitroaromatic vapours detection at room-temperature *Sens. Actuators, B* **2010**, *151*, 191– 197
17. Ahmad, R. K.; Parada, A. C.; Hudziak, S.; Chaudhary, A.; Jackman, R. B. Nanodiamond-coated silicon cantilever array for chemical sensing *Appl. Phys. Lett.* **2010**, *97*, 093103
18. Gruber, A.; Dräbenstedt, A.; Tietz, C.; Fleury, L.; Wrachtrup, J.; von Borczyskowski, C. Scanning confocal optical microscopy and magnetic resonance on single defect centers *Science* **1997**, *276*, 2012
19. Treussart, F.; Jacques, V.; Wu, E.; Gacoin, T.; Grangier, P.; Roch, J.-F. Photoluminescence of single colour defects in 50 nm diamond nanocrystals *Physica B* **2006**, *376–377*, 926– 929
20. Nesvizhevsky, V.; Cubitt, R.; Lychagin, E.; Muzychka, A.; Nekhaev, G.; Pignol, G.; Protasov, K.; Strelkov, A. Application of diamond nanoparticles in low-energy neutron physics *Materials* **2010**, *3*, 1768– 1781
21. Krueger, A.; Lang, D. Functionality is key: recent progress in the surface modification of nanodiamond *Adv. Func. Mat.* **2012**, *22*, 890– 906
22. Portet, C.; Yushin, G.; Gogotsi, Y. Electrochemical performance of carbon onions, nanodiamonds, carbon black and multiwalled nanotubes in electrical double layer capacitors *Carbon* **2007**, *45*, 2511– 2518
23. Pech, D.; Brunet, M.; Durou, H.; Huang, P.; Mochalin, V.; Gogotsi, Y.; Taberna, P. L.; Simon, P. Ultrahigh-power micrometre-sized supercapacitors based on onion-like carbon *Nature Nanotechnol.* **2010**, *5*, 651– 654
24. Girard, H. A.; Perruchas, S.; Gesset, C.; Chaigneau, M.; Vieille, L.; Arnault, J. C.; Bergonzo, P.; Boilot, J. P.; Gacoin, T. Electrostatic grafting of diamond nanoparticles: a versatile route to nanocrystalline diamond thin films *ACS Appl. Mater. Interfaces* **2009**, *1* (12) 2738– 2746
25. Kozak, H.; Kromka, A.; Babchenko, O.; Rezek, B. Directly grown nanocrystalline diamond field-effect transistor microstructures *Sensor Lett.* **2010**, *8*, 482– 487
26. Kromka, A.; Rezek, B.; Remes, Z.; Michalka, M.; Ledinsky, M.; Zemek, J.; Potmesil, J.; Vanecek, M. Formation of continuous nanocrystalline diamond layers on glass and silicon at low temperatures *Chem. Vap. Deposition* **2008**, *14*, 181– 186

27. Arnault, J. C.; Saada, S.; Williams, O. A.; Haenen, K.; Bergonzo, P.; Nesladek, M.; Polini, R.; Osawa, E. Diamond nanoseeding on silicon: stability under H₂ MPCVD exposures and early stages of growth *Diam. Relat. Mater.* **2008**, *17*, 1143– 1149
28. Dykman, L.; Khlebtsov, N. Gold nanoparticles in biomedical applications: Recent advances and perspectives *Chem. Soc. Rev.* **2012**, *41*, 2256– 2282
29. Daniel, M. C.; Astruc, D. Gold nanoparticles: Assembly, supramolecular chemistry, quantum-size-related properties, and applications toward biology, catalysis and nanotechnology *Chem. Rev.* **2004**, *104*, 293– 346
30. Arnault, J. C.; Petit, T.; Girard, H.; Chavanne, A.; Gesset, C.; Sennour, M.; Chaigneau, M. Surface chemical modifications and surface reactivity of nanodiamonds hydrogenated by CVD plasma *Phys. Chem. Chem. Phys.* **2011**, *13*, 11481– 11487
31. Girard, H. A.; Arnault, J. C.; Perruchas, S.; Saada, S.; Gacoin, T.; Boilot, J. P.; Bergonzo, P. Hydrogenation of nanodiamonds using MPCVD: a new route toward organic functionalization *Diam. Relat. Mater.* **2010**, *19*, 1117– 1123
32. Petit, T.; Arnault, J. C.; Girard, H. A.; Sennour, M.; Bergonzo, P. Early stages of surface graphitization on nanodiamond probed by X-ray photoelectron spectroscopy *Phys. Rev. B* **2011**, *84*, 233407
33. Osswald, S.; Yushin, G.; Mochalin, V.; Kucheyev, S. O.; Gogotsi, Y. Control of sp²/sp³ carbon ratio and surface chemistry of nanodiamond powders by selective oxidation in air *J. Am. Chem. Soc.* **2006**, *128*, 11635– 11642
34. Kolíbal, M.; Konečný, M.; Ligmajer, F.; Škoda, D.; Vystavěl, T.; Zlámal, J.; Varga, P.; Šikola, T. Guided assembly of gold colloidal nanoparticles on silicon substrates prepatterened by charged particle beams *ACS Nano* **2012**, *6*, 10098– 10106
35. Sugimura, H.; Ishida, Y.; Hayashi, K.; Takai, O.; Nakagiri, N. Potential shielding by the surface water layer in Kelvin probe force microscopy *Appl. Phys. Lett.* **2002**, *80*, 1459
36. Hornauer, H.; Vancea, J.; Reiss, G.; Hoffmann, H. Thickness dependence of the work function in double-layer metallic films *Z. Phys. B – Condensed Matter* **1989**, *77*, 399– 407
37. Jacobs, H. O.; Leuchtmann, P.; Homan, O. J.; Stemmer, A. Resolution and contrast in Kelvin probe force microscopy *J. Appl. Phys.* **1998**, *84*, 3
38. Rezek, B.; Garrido, J. A.; Stutzmann, M.; Nebel, C. E.; Snidero, E.; Bergonzo, P. Local oxidation of hydrogenated diamond surfaces for device fabrication *Phys. Stat. Sol. (a)* **2002**, *193*, 523– 528
39. Elias, G.; Glatzel, T.; Meyer, E.; Schwarzman, A.; Boag, A.; Rosenwaks, Y. The role of the cantilever in Kelvin probe force microscopy measurements *Beilstein J. Nanotechnol.* **2011**, *2*, 252– 260
40. Sadewasser, S.; Jelinek, P.; Fang, Ch-K.; Custance, O.; Yamada, Y.; Sugimoto, Y.; Abe, M.; Morita, S. New insights on atomic-resolution frequency-modulation Kelvin-probe force microscopy imaging of semiconductors *Phys. Rev. Lett.* **2009**, *103*, 266103
41. Takeuchi, D.; Riedel, M.; Ristein, J.; Ley, L. Surface band bending and surface conductivity of hydrogenated diamond *Phys. Rev. B* **2003**, *68*, 041304(R)
42. Takeuchi, D.; Yamanaka, S.; Watanabe, H.; Okushi, H. Device grade B-doped homoepitaxial diamond thin films *Phys. Stat. Sol. (a)* **2001**, *186*, 269– 280
43. Verveniotis, E.; Kromka, A.; Ledinský, M.; Rezek, B. How nanocrystalline diamond films become charged in nanoscale *Diam. Relat. Mater.* **2012**, *24*, 39– 43
44. Kawarada, H. Hydrogen-terminated diamond surfaces and interfaces *Surf. Sci. Rep.* **1996**, *26*, 205– 209

45. Tachiki, M.; Kaibara, Y.; Sumikawa, Y.; Masatsugu, S.; Kanazawa, H.; Banno, T.; Song, K. S.; Umezawa, H.; Kawarada, H. Characterization of locally modified diamond surface using Kelvin probe force microscope *Surf. Sci.* **2005**, 581, 207– 212
46. Cui, J. B.; Ristein, J.; Ley, L. Low-threshold electron emission from diamond *Phys. Rev. B* **1999**, 60, 23
47. Verveniotis, E.; Čermák, J.; Kromka, A.; Ledinský, M.; Remeš, Z.; Rezek, B. Local electrostatic charging differences of sub-100 nm nanocrystalline diamond films *Phys. Stat. Sol. (a)* **2010**, 207, 2040– 2044
48. Jelínek, P.; Pérez, R.; Ortega, J.; Flores, F. Hydrogen dissociation over Au nanowires and the fractional conductance quantum *Phys. Rev. B* **2006**, 96, 046803
49. Valden, M.; Lai, X.; Goodman, D. W. Onset of catalytic activity of gold clusters on titania with the appearance of nonmetallic properties *Science* **1998**, 281 (5383) 1647– 1650